Structural study of low concentration LiCl aqueous solutions in the liquid, supercooled, and hyperquenched glassy states

K. Winkel,[1] M. Seidl,[1] T. Loerting,[1] L. E. Bove,[2] S. Imberti,[3] V. Molinero,[4] F. Bruni,[5] R. Mancinelli,[5] and M. A. Ricci[5,a)]

[1]*Institute of Physical Chemistry, University of Innsbruck, Innrain 52a, 6020 Innsbruck, Austria*
[2]*IMPMC, Université P. et M. Curie et CNRS-UMR, 7590 Paris, France*
[3]*STFC, ISIS Facility, STFC Rutherford Appleton Laboratory, Harwell Science and Innovation Campus, Didcot, Oxon OX11 0QX, United Kingdom*
[4]*Department of Chemistry, University of Utah, Salt Lake City, Utah 84112, USA*
[5]*Dipartimento di Fisica "E. Amaldi," Università degli Studi "Roma Tre," Via della Vasca Navale 84, 00146 Roma, Italy*

(Received 10 September 2010; accepted 24 November 2010; published online 12 January 2011)

Neutron diffraction experiments on a solution of LiCl in water ($R = 40$) at ambient conditions and in the supercooled and hyperquenched states are reported and analyzed within the empirical potential structure refinement framework. Evidence for the modifications of the microscopic structure of the solvent in the presence of such a small amount of salt is found at all investigated thermodynamic states. On the other hand, it is evident that the structure of the hyperquenched salty sample is similar to that of pure low density amorphous water, although all the peaks of the radial distribution functions are broader in the present case. Changes upon supercooling or hyperquenching of the ion's hydration shells and contacts are of limited size and evidence for segregation phenomena at these states does not clearly show up, although the presence of water separated contacts between ion of the same sign is intriguing. © *2011 American Institute of Physics*. [doi:10.1063/1.3528000]

I. INTRODUCTION

Amorphous polymorphism (polyamorphism) is one of the key concepts in our current understanding of water, its structure, physical properties, and anomalies.[1–5] The basic idea is that liquid water at ambient conditions (average density = 1.00 g/cm^3) is constantly fluctuating between high-density domains and low-density domains.[6] The high- and low-density domains cannot be isolated at ambient conditions, but it may be possible to obtain phase segregation in the deeply supercooled regime at temperatures below 235 K. Unfortunately, experiments on bulk water cannot be done in this temperature region because of the homogeneous nucleation limit and rapid crystallization, which prevents supercooling of liquid water below 235 K (in the so-called "no-man's land").[7] One way of avoiding rapid crystallization is by cooling water at rates which even exceed the crystallization rate (hyperquenching). Samples are typically cooled to 77 K, at cooling rates up to 10^7 K/s (Ref. 8) and a vitrified, glassy state of matter is eventually obtained. Interestingly, hyperquenched glassy water has a density of ~0.92 g/cm^3, representing a low-density form of noncrystalline water, often also referred to as low-density amorphous ice (LDA). Thus we could infer that upon hyperquenching the low-density domain structure is preferred over the high-density domain structure. Devitrification, i.e., the transition from the glass to the deeply supercooled liquid, was found to take place close to $T_g \sim 136$ K; above this temperature, a sudden increase in heat capacity,[9] isotope mixing of layers,[10] and sudden penetration of an indentor into the sample[11] were reported. Unfortunately, these samples crystallize above approximately 150 K, leaving a rather narrow window for experiments on deeply supercooled water, at ambient pressure. Upon applying pressure LDA transforms to the high-density amorphous form of ice (HDA), with density of 1.15 g/cm^3 at ambient pressure.[12] This transition takes place suddenly in a first orderlike manner at ~700 MPa at 77 K and ~450 MPa at 125 K.[13] Interestingly it has been argued that, with increasing pressure, the microscopic structure of supercooled water evolves from a low-density liquid, similar to LDA, to a high-density phase, similar to HDA.[14] While in pure water the existence of the no-man's land prevents a direct experimental answer of the question whether or not the glassy states of water are thermodynamically continuously connected to ambient water, the continuity can be shown in aqueous solutions in the pressure range up to 200 MPa. In this manner the study of aqueous solutions at low temperatures is inevitably connected to polyamorphism.[15]

Introduction of a small amount of salt solutes has been shown to affect the structure of water in a manner similar to the application of high pressures.[16–18] Conversely, introduction of a large amount of solute results in partial destruction of the topological elements found in bulk water due to the increasing number of incomplete hydration shells. Thus the transition from dilute to concentrated solutions is typically put at a ratio of solute:water molecules = 1:20 ($R = 20$). In the case of LiCl, concentrated solutions ($R \leq 12$) can easily be vitrified by use of conventional cooling of rates up to 10^2 K/s, without the need for hyperquenching techniques, while for dilute solutions of $R \geq 15$ vitrification requires high rates and hyperquenching.[19,20] In this work we choose to study dilute

a)Electronic mail: riccim@fis.uniroma3.it.

aqueous solutions of LiCl at $R = 40$, for the reasons given below. A very interesting aspect is that the glass-to-liquid transition temperature T_g shows a highly nonlinear dependence on solute concentration (see Fig. 3 in Ref. 20). Initial increase of solute concentration from $R = \infty$ (pure water) to $R = 40$ results in a decrease of T_g from 136 to 129 K. Further increase from $R = 40$ to $R = 15$ results first in a slow increase, followed by a sudden increase at $R = 21$ from 132 to 142 K. That is, there is a T_g-minimum at $R = 40$ and a maximum at $R = 18$. Since materials at their T_g's are considered to be in an isoviscous state, a minimum in T_g implies a minimum in viscosity (as a function of composition at fixed temperature).[20] Thus in the case of LiCl solutions, at $R = 40$ the maximally plasticized state of the water network and the maximum of water fluidity is attained. It is conceivable that the occurrence of this state of maximum fluidity is related to polyamorphism in aqueous solutions, and hence it is important to investigate this state further. In addition to the minimum in T_g also the increase in heat capacity at T_g (Δc_p) shows a minimum; as a consequence, the low-density configuration can be labeled as "strong glass former," according to the Angell's scheme.[21]

Suzuki and Mishima have even shown that dilute glassy solutions can be phase separated into two parts: a highly concentrated solution of LiCl, which may in a way resemble HDA, and low-density glassy water,[22] which resembles LDA. This phase separation may go hand in hand with an increase in ion-pairing, which was found earlier in the glassy state,[23] or with other clear changes of the microscopic structure of water. In the case of LiCl the T_g minimum and the subsequent sharp T_g rise are much more pronounced than in other chlorides such as NaCl, CsCl, or $MgCl_2$ (see Fig. 7 in Ref. 24). While all lithium-halides show this type of behavior, the minimum and the sharp rise are most pronounced in LiCl (see Fig. 6 in Ref. 24). We, therefore, report here a structural study of LiCl solutions ($R = 40$) in the glassy state, in the metastable (supercooled) liquid state, and in the stable liquid state, with the major aim of comparing especially the water–water radial distribution functions (RDFs) with pure hyperquenched glassy water (HGW) and furthermore to analyze ion–water and ion–ion interaction for checking for increase in ion-pairing at low temperatures. There is one thing that we want to emphasize at the outset: future work at different solute:water ratios (e.g., at $R = 30$, 18, and 10) will be necessary to learn more about the structural aspects underlying the unexpected behavior of the glass transition temperature as a function of R.

II. EXPERIMENT AND DATA REDUCTION

A. Sample preparation

The LiCl–water (–heavy water) solution was prepared from Sigma anhydrous LiCl (99.98%) dissolved in deionized distilled water (heavy water) in the appropriate proportion ($R = 40$) under Ar atmosphere. The two mixtures have been mixed under Ar atmosphere in the appropriate proportion in order to obtain a 50% H/D mixture. The solutions have been filtered through a 0.2 μm nanoporous filter and stored into cylindrical glass tubes flame sealed. The tubes were kept in liquid nitrogen during sealing in order to avoid water evaporation. The concentration of the three samples has been checked by the "Service Central d'Analyse du CNRS (SR-59)."

To form a glassy state of dilute LiCl aqueous solution, high cooling rates are necessary.[20] Therefore the hyperquenching technique was used.[8] The hyperquenched samples were prepared as described in Ref. 25 for pure water (HGW). Micrometer-sized droplets were made with an ultrasonic nebulizer operating at 3 MHz (LKB Instruments, model 108, with the parameters 80% H_2O, 4 l/min, N_2 carrier gas 2.0 l/min). The aerosol was transferred with nitrogen (purity of 99.995%) as carrier gas through a silicon tube which is cooled with ice water in order to reduce the relative amount of water vapour. The aerosol enters the vacuum chamber through an aperture of 300 μm diameter and is deposited on a cryoplate (Cu) at 77 K. Deposition time varied between 70 and 80 min.

B. Neutron diffraction experiment

The experiment has been performed at the SANDALS diffractometer,[26] installed at the ISIS pulsed neutron source (UK). Liquid samples were contained into standard Ti–Zr flat cells of $t = 1$ mm internal thickness and 1 mm wall thickness, while cells with $t = 2$ mm were used for the HGW samples. Sample containers were connected to a He cryostat for the temperature control. Measurements on the liquid samples have been performed at $T = 298$ K (ambient) and $T = 268$ K (supercooled), while the hyperquenched sample (HGW), after storage and recovery in liquid nitrogen, has been measured at $T = 80$ K. In order to apply the H/D contrast method in the neutron diffraction experiment, water hydrogens have been isotopically substituted (see Sec. II A) and measurements have been performed at each temperature on three different isotopic mixtures: i.e., one fully deuterated, one fully protonated, and an equimolar mixture of the two (hereafter labeled HDO) in the case of liquid samples, while the deuterated sample was contaminated during the hyperquenching procedure and its D/H ratio was 3:1. For each sample, data have been accumulated for about 8–10 h, with ISIS running on average at 180 μA; measurements have also been performed for the empty containers, empty instrument, empty cryostat, and a standard vanadium slab ($5.0 \times 5.0 \times 0.348$ cm^3).

C. Data reduction

Data reduction has been performed by using the suite of programs (GUDRUN) (Ref. 27) available for SANDALS and widely described elsewhere.[28] This performs corrections for multiple scattering, absorption, and inelasticity effects, subtracts the sample container contribution, and normalizes the data to an absolute scale. GUDRUN also performs a check of the sample density, ρ, and composition against the high Q limit of the total measured differential scattering intensity, defined as

$$\lim_{Q\to\infty} I(Q) = \frac{\rho t \sum_{\alpha} c_\alpha \sigma_\alpha}{4\pi}, \tag{1}$$

where Q is the modulus of the exchanged momentum and c_α and σ_α are the fraction and total scattering cross sections[29]

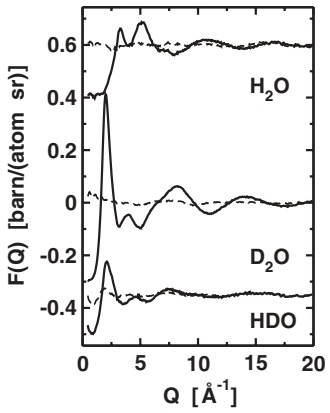

FIG. 1. Measured differential cross sections of three LiCl–water solutions ($R = 40$) at ambient temperature (solid line), along with the residuals of the EPSR fit (dashed lines). Data have been offset for clarity.

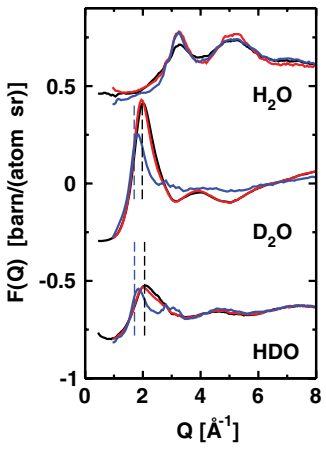

FIG. 2. The measured differential cross sections of three isotopically substituted LiCl aqueous solutions ($R = 40$) at different temperatures, namely, at ambient temperature (black line), in the supercooled liquid state (red line), and in the HGW state (blue line). The vertical dashed lines indicate the position of the first diffraction peak of pure D_2O and pure HDO at ambient conditions (Ref. 45) (black dashed); the blue dashed lines indicate the position of the same peaks in a pure HGW sample (Ref. 46). Data have been offset for clarity.

of atoms of type α. In the case of the hyperquenched samples, this level is used to establish the fraction of void volume in the sample container, assuming for the sample a density of 0.0934 atoms/Å^3. This density value has been calculated from the density of pure HGW (0.094 atoms/Å^3), taking into account the ratio between the molar mass of the solution and pure water, and double checked against the shift of the first halo peak in the x-ray diffraction pattern (not shown) of HGW–LiCl compared to amorphous ices with different densities.

The final output of the data reduction procedure is the neutron differential cross section (DCS):

$$F(Q) = \sum_{\alpha} \sum_{\beta>\alpha} c_\alpha c_\beta b_\alpha b_\beta (2 - \delta_{\alpha\beta})(S_{\alpha\beta}(Q) - 1), \qquad (2)$$

where b_α is the neutron coherent scattering length[29] of the α species. $S_{\alpha\beta}$ is the partial structure factor (PSF), namely, the Fourier transform of the RDF of the α, β pair,

$$S_{\alpha\beta}(Q) = 1 + 4\pi\rho \int_0^\infty r^2 (g_{\alpha\beta}(r) - 1) \frac{\sin(Qr)}{Qr} dr. \qquad (3)$$

Since hydrogen and deuterium have markedly different scattering lengths, the H/D substitution on the solvent gives access to three independent DCS data sets, characterized by a good contrast one to each other (see Fig. 1).

A LiCl–water solution consists of $m = 4$ different atomic species (namely, H/D, O, Li, and Cl); consequently, each DCS is the combination of $m(m + 1)/2 = 10$ distinct PSFs and complete exploitation of the microscopic structure of this solution is subject to the inversion of a system of three equations with ten unknowns [see Eq. (2)], which are the individual PSFs. The solution of this inversion is not unique and can only be performed with the support of a proper computer simulation model and based on complementary knowledge, such as for instance molecular geometry of water, presence of H-bonds between water molecules, and ionic charges. In the present instance we have used the empirical potential structure refinement (EPSR) (Ref. 30–32) code. Applications of this code to studies of aqueous solutions are thoroughly described in Refs. 16, 17, 28, and 33–40. Briefly, this is a standard Monte Carlo simulation of the solution in question, which iteratively adjusts a perturbation to the starting reference potential until the simulated DCS converges to a satisfactory fit of the measured data. This is usually achieved after hundreds of iterations, provided that the starting reference potential can mimic the relevant features of the system, such as the presence of a network of H-bonds in the present instance. Several different choices of this potential model may be reasonable, and many are available in the literature at least for water; nevertheless, the experience over the years has demonstrated that the different choices do not dramatically affect the final result, when used within the EPSR code.[41,42] In particular the range of RDF compatible with the experimental data is usually rather narrow, although the degree of reliability of the individual RDF depends, of course, on its weight within the DCS functions. Specifically at low solute concentrations, water–water RDFs will have the higher weight, followed by solute–water ones, while solute–solute terms will give the lower contribution to the measured DCS. After convergence to a good fit, the EPSR simulation proceeds by accumulating molecular configurations compatible with the data. These are finally used to evaluate the whole set of site–site RDF, along with other structural properties of interest, as. for instance. the distribution of H-bonds. Consequently the DCSs reported in Figs. 1 and 2 are experimental data, while the RDFs discussed in the following sections are the results of the EPSR simulations. A detailed discussion about their uniqueness and comparison with other inversion techniques, such as reverse Monte Carlo, can be found in Refs. 30–32, 41, and 42.

For the present solutions, we have used as reference potential the simple point charge/extended model[43] for water–water interactions and Lennard-Jones plus fractional charges for the solutes,[44] according to Table I. The Lorentz Berthelot rules have been applied for the interaction between different species. The simulation box dimensions and composition are reported in Table I for the liquid and hyperquenched (HGW) samples.

TABLE I. Lennard-Jones parameters and effective atomic charges used to start the EPSR refinement of the neutron diffraction data, taken from Ref. 43 and Refs. 36 and 44 for water and LiCl, respectively. Sample density and size of the EPSR simulation box, along with the number of water molecules, Li^+, and Cl^- ions in the box, are reported in the bottom part of the table. HGW labels the hyperquenched sample.

Atom	ϵ(kJ/mol)	σ(Å)	$q(e)$		
O	0.65	3.166	−0.8476		
H	0.00	0.000	0.4238		
Li	0.69	1.500	1.0000		
Cl	0.57	4.200	−1.0000		
Sample	density (atoms/Å^3)	L_{box} (Å)	H_2O	Li^+	Cl^-
liquid	0.0992	26.42	600	15	15
HGW	0.0934	26.96	600	15	15

The quality of the fits obtained for the present data is shown in Fig. 1, where the DCS functions for ambient temperature samples are reported along with the residuals of the corresponding EPSR simulation. The fits at the other thermodynamic states are of the same quality.

III. RESULTS AND DISCUSSION

A. Differential cross sections

It is instructive to comment on the behavior with temperature of the DCS data, before looking and commenting EPSR results in r-space. These data (see Fig. 2) show indeed clear trends with temperature and differences with the case of pure water,[45,46] which are worth to be described. The DCS of pure H_2O is characterized by a double peak in the range 3–6 Å^{-1}: the position of the two maxima does not sensibly change going from ambient to the HGW state, while their relative intensity changes. The same behavior is found in the case of the LiCl solution, with the intensity of the first peak increasing in the supercooled and in the HGW states. The HDO mixture in pure ambient water has an asymmetric first peak at ∼2.06 Å^{-1}, which moves to smaller Q-values on lowering the temperature and goes to 1.71 Å^{-1} in the HGW state. In our sample this peak comes at $Q = 2.11$ Å^{-1} at ambient temperature, moves to ∼2 Å^{-1} in the supercooled state, and reaches $Q = 1.83$ Å^{-1} in the HGW sample. Interestingly both our HGW data and those of Ref. 46 show that the first peak of the DCS sharpens and develops a secondary structure at 2.8–2.9 Å^{-1} in the glassy state. As far as the D_2O data are concerned, in pure water the first peak (at 1.98 Å^{-1} at ambient conditions) moves to smaller Q-values upon supercooling and goes to 1.7 Å^{-1} in the HGW sample. We notice the same trend in the LiCl solution, with the peak at 2.02 Å^{-1} at ambient temperature, moving to 1.92 Å^{-1} in the supercooled state. Our HGW sample is, as already noticed, contaminated by H_2O; thus, the comparison with pure deuterated HGW is not completely appropriate; the misfit with DCS data of the other two samples at Q-values larger than 4 Å^{-1} is also due to contamination. We stress that contamination does not however spoil our simulation results, since the simulation box of the HGW sample has been built using the real sample composition.

In summary, the DCS data of the LiCl aqueous solutions show the same temperature behaviors as pure water ones, as far as shift and peak intensity are concerned. Nevertheless the first peaks of HDO and D_2O samples at ambient conditions are at larger Q-values than in pure water and do not reach the same positions when the sample is hyperquenched. Since the DCS signals at the present solute concentration are dominated by the water contribution, these findings are the signature of differences in the microscopic arrangement of water molecules in the solution compared to neat water: possibly the same differences which depress the crystal nucleation temperature of the solution.

B. Water–water radial distribution functions

In pure ambient water the almost tetrahedral network of H-bonds is manifested by the position of the first two peaks of the $g_{OO}(r)$ at 2.8 and 4.5 Å, respectively. Solvation of ions is known to affect the position of the second peak, while leaving almost unperturbed the first one,[34] in a manner similar to the application of an external pressure. The present LiCl solution confirms this finding (see Fig. 3), with the second peak at 3.9 Å, corresponding to an equivalent pressure of 307 MPa. On lowering the temperature the first peak moves to shorter distances (this is best visible in the HGW sample), as found also in pure water,[47] while the second one goes to larger distances. This suggests that at lower temperatures the network tends to recover tetrahedrality, although the second neighbor shell in our HGW sample is closer to the first one compared to pure HGW (Ref. 46) (see Fig. 4). We notice also that the salty HGW looks less ordered than the pure water one, with less intense and broader peaks of all three RDFs.

When pure water is supercooled, the $g_{HH}(r)$ shows very little changes,[47] on the contrary in this solution we notice that both peak position and intensity change on supercooling (see Fig. 3), with the two main peaks going far apart in the HGW

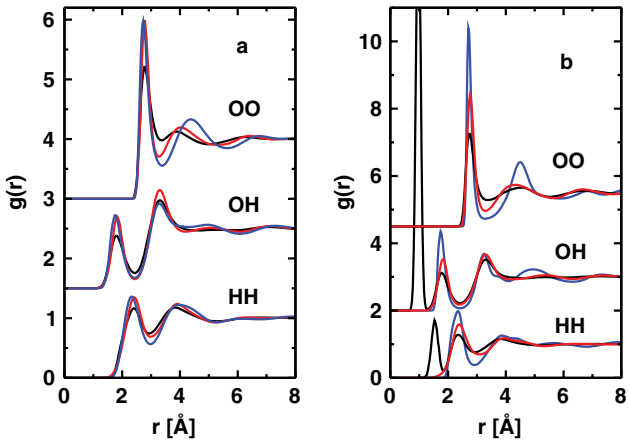

FIG. 3. The EPSR calculated radial distribution functions of water atoms in LiCl ($R = 40$) solution (a) and in pure water (b). As in Fig. 2, data at ambient conditions are reported in black, those in the supercooled state in red, and finally the HGW data in blue. Data for OO and OH pairs have been offset for clarity. Note that in the case of pure ambient water also, the intramolecular peaks have been reported. Data for pure water are from Ref. 31, 46, and 47, respectively.

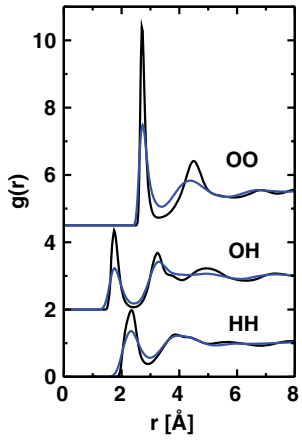

FIG. 4. The EPSR calculated radial distribution functions of water atoms in the hyperquenched glassy state, in the LiCl solution (blue), and in pure water (black) (Ref. 46). Data for OO and OH pairs have been offset for clarity.

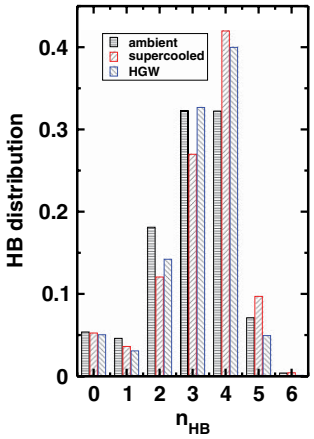

FIG. 5. Distribution function of the hydrogen bonds at the three investigated state points. Two water molecules are considered H-bonded when the H site of the second molecule sticks by the oxygen of the first one within a distance shorter than or equal to the position of the first minimum of the $g_{OH}(r)$.

sample. The peak positions for this sample are the same as for pure HGW (Ref. 46) (see Fig. 4), but the first peak is less intense and broader.

In pure water supercooling is associated with the sharpening of the first peak of the $g_{OH}(r)$,[47] that is the signature of increased directionality of the H-bonds. In the salty sample instead both first and second peaks become sharper, and additionally their intensities increase (see Fig. 3). Moreover the first peak moves to shorter distances with hyperquenching, suggesting a shortening of the H-bonds, while the intensity of the second peak decreases. The position of the first peak is the same as for pure HGW (Ref. 46) (see Fig. 4), although the peak width is almost twice and the second neighbor shell is centered at larger distances. We notice also that the second peak is overall broader and does not show the shoulder at ∼3.74 Å, which characterizes pure HGW.

Due to the above reported changes of the RDF, the average number of neighboring oxygens around a water molecule decreases with temperature from 4.3 ± 1.1 at ambient conditions to 4.0 ± 1.0 in the supercooled state and 3.70 ± 0.91 in the HGW sample,[48] while the average number of H-bonds, as calculated from the distribution functions reported in Fig. 5, increases from 3.0 to 3.2–3.3 in the supercooled and HGW samples.

All above findings are consistent with an increase of the H-bond strength and average number, with consequent reduction of non-H-bonded molecules within the mesh of the H-bond network (the so-called interstitial molecules), on going from ambient to the supercooled and hyperquenched states. In particular the peak positions of the RDFs of the HGW sample are identical to those of the pure HGW, although the overall broadness of the peaks in the salty sample suggests that the presence of salts determines a higher degree of disorder in the structure. Overall, the radial distribution functions of salty water are broader than those of neat water, but their temperature behavior is similar.

C. Li^+ hydration shell

The Li^+ hydration shell is well defined and stable with temperature, with average distances of 1.95 and 2.64 Å for the Li–O and Li–H pairs (see Fig. 6). These distances are compatible with a close alignment of the O–Li director with the water dipole, as already found in the case of aqueous solutions of LiOH.[36] We notice however that in the present case the Li–O distance is shorter than it was in the hydroxide solution; this difference might be due to the lower solute concentration of the present sample, as suggested by the weak concentration dependence of the cation–oxygen distance evidenced in Ref. 36. We notice also that *ab initio* simulations of a Li^+ ion in a box with 32 water molecules[49] predict a Li–O distance even shorter than that found here. The number of water oxygens in the Li^+ hydration shell is of the order of 4 and shows a weak temperature dependence (3.91 ± 0.49, 3.80 ± 0.40, and 3.79 ± 0.45 for ambient, supercooled, and HGW samples,

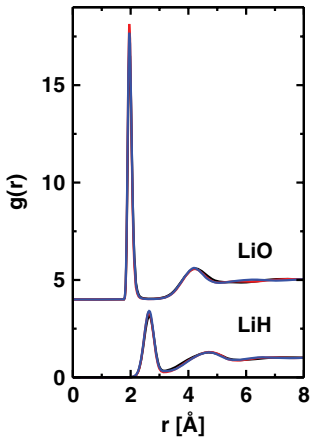

FIG. 6. The EPSR calculated radial distribution functions of water atoms around a Li^+ ion (same colors as in Fig. 2). Data have been offset for clarity. The first sharp peaks of the two radial distribution functions define the Li^+ hydration shell, formed by about four water molecules.

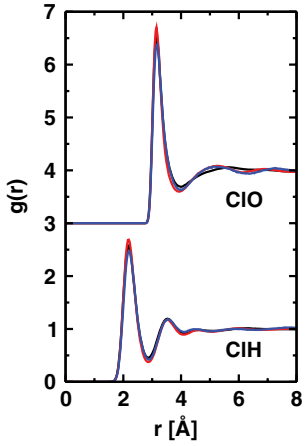

FIG. 7. The EPSR calculated radial distribution functions of water atoms around a Cl^- ion (same colors as in Fig. 2). Data have been offset for clarity. The first intense peaks of the two radial distribution functions define the Cl^- hydration shell, formed by about six water molecules.

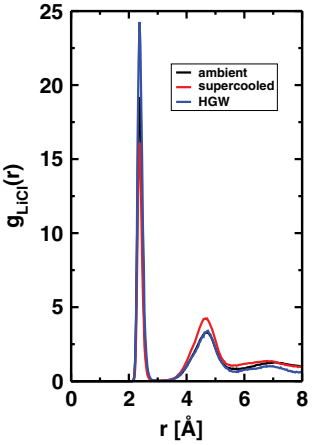

FIG. 8. EPSR calculated radial distribution function of the Li^+–Cl^- pair (same colors as in Fig. 2). In spite of the high intensity of the first peak, the number of ion–ion contacts is negligible at this concentration at all temperatures.

respectively), which however has no statistical relevance and cannot be considered as a signature of phase separation.

D. Cl^- hydration shell

Each Cl^- ion accommodates about six water hydrogens in its hydration shell (precisely 6.0 ± 1.3, 6.0 ± 1.2, and 5.5 ± 1.3 for ambient, supercooled, and HGW samples, respectively) and between eight and seven oxygens. Although these numbers show a trend with temperature, their statistical uncertainty does not allow to claim about phase separation. The Cl–H and Cl–O shells (see Fig. 7) are centered at 2.18 and 3.15 Å at ambient conditions, i.e., at slightly shorter distances compared with the findings of Jal *et al.*[50] at higher salt concentration, by first difference neutron diffraction.

The present data confirm that the hydration shell of Cl^- in salt solutions is shorter than that found in acidic solutions.[17,39] Interestingly, for the HGW sample both Cl–H and Cl–O distances increase, allowing a better Cl–H–O alignment.

E. Ion contacts

The $g_{\mathrm{LiCl}}(r)$, reported in Fig. 8, shows a very sharp, intense peak at 2.37 Å due to Li–Cl contacts, followed by a second peak at ∼4.7 Å, which corresponds to ∼1 water separated Li–Cl pair. The number of direct contacts, calculated as $n(r) = \int 4\pi\rho r^2 g_{\mathrm{LiCl}}(r)\,dr$ over the first peak, is between 0.2 and 0.3 per ion, with an uncertainty of ±0.4, meaning that recombination is a rare event at this solute concentration and thermodynamic states.

The $g_{\mathrm{LiLi}}(r)$ and $g_{\mathrm{ClCl}}(r)$ functions (see Fig. 9) show an interesting behavior with temperature. In particular, $g_{\mathrm{ClCl}}(r)$ shows two neighboring shells at ∼5 and ∼7 Å and only in the HGW sample the presence of a prepeak at ∼4 Å due to water separated contacts. The presence of water separated pairs is evident at all temperatures in the $g_{\mathrm{LiLi}}(r)$ function, where a small prepeak at ∼3.7 Å is already visible at ambient conditions and becomes an intense peak in the supercooled and HGW phases. It is not clear however if this phenomenon may be the signature of the onset, by lowering the temperature, of the phase separation predicted at higher pressures.[51,52]

IV. CONCLUSIONS AND OUTLOOK

We have studied the structure of dilute aqueous solutions of LiCl using neutron diffraction experiments at ambient conditions (298 K), in the supercooled state (268 K), and in the hyperquenched glassy state (80 K). A ratio $LiCl:H_2O = 1:40$ ($R = 40$) was employed because at this dilution level LiCl solutions are known to be of the highest fluidity at 130 K. Interestingly, the glass-to-liquid transition temperature T_g at this dilution is lower by a few Kelvin compared even to pure water.[20] By contrast, the state of the lowest fluidity showing a T_g by a few Kelvin higher compared to that of pure water is found at a ratio of $R = 18$, which is subject to future investigation. It may be possible that this unusual behavior of

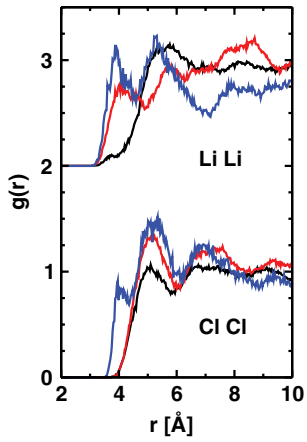

FIG. 9. EPSR calculated cation–cation and anion–anion radial distribution functions (same colors as in Fig. 2), showing the presence of water separated contacts at about 4 Å in the HGW sample and in the case of Li^+ also in the supercooled liquid. Data have been offset for clarity.

a maximum and minimum in T_g is related to the occurrence of a changing fraction of LDA and HDA like configurations.

Upon lowering the temperature, the differential cross sections of LiCl aqueous solutions at $R = 40$ show the same trends as pure water, but the radial distribution functions of water, as for other salt solutions, are distorted with respect to those of the neat solvent. In particular, at ambient conditions, ions solvation determines a shrinkage of the second neighbor's shell and a consequent loss of tetrahedrality, and the HGW phase can be associated with the LDA state of water, but not the HDA state. Indeed on lowering the temperature through the supercooled phase to the HGW one, we notice that the H-bonds recover linearity and the network tetrahedrality increases. The structure of the salty HGW is similar to that of the pure HGW, although all the peaks of the radial distribution functions are broader, suggesting that the distortions induced by the salt on the structure of water persist in this state and determine a variety of different local configurations within the H-bond network. The number of neighboring water molecules decreases upon cooling and in the HGW phase, thus confirming that this amorphous form of the solution can be associated with the LDA polymorph of water.

Changes of the hydration shell of the ions are little and there is also little or no evidence for phase separation. Indeed the number of direct or water separated ion contacts does not show a statistically relevant increase in the HGW phase, although a peak ascribable to water separated cation–cation and anion–anion contacts shows up in the HGW sample. That ions of the same sign are brought closer to each other is an intriguing issue, which merits further investigation from both experimental and computational sides.

We want to emphasize that separation into two distinct glasses, and a double-glass transition phenomenon has been observed in LiCl solutions vitrified at high pressures,[51,52] by pressure-induced amorphization[53] or pressure-induced vitrification.[54] The water-rich phase resembles the HDA phase of bulk water,[52] and, therefore, we plan to investigate the difference between the low-pressure forms to the high-pressure forms of the $R = 40$ solution in the future. This HDA phase can be converted to the LDA phase in LiCl solutions of $R = 20$ by decompressing the vitrified high-density state at 142 K to 0.1 GPa.[55] This decompression-induced HDA→LDA transition is highly similar to the phase-transitions incurred upon decompressing bulk HDA, without any salt, at similar temperatures.[56,57] The role of annealing on the phase separation is another issue which deserves consideration in future experiments.

ACKNOWLEDGMENTS

The experiments on SANDALS have been performed within the agreement between CCLRC and CNR, concerning collaboration in scientific research at the spallation neutron source ISIS and with partial financial support of CNR. We would like to thank D. T. Bowron for providing the data on HGW water, reported in Figs. 3 and 4 and A. P. Russo of the Dipartimento di Fisica "E. Amaldi" (Università degli studi Roma Tre) for computer support. We are grateful for financial support from the European Research Council (T.L., Starting Grant SULIWA), Austrian Academy of Sciences (M.S., DOC-fellowship), Austrian Science Fund FWF (K.W., Hertha Firnberg position), "Italien Zentrum" of the University of Innsbruck (K.W.), and Young Investigators Program of the Beckman Foundation (V.M.).

[1] O. Mishima and H. E. Stanley, Nature (London) **396**, 329 (1998).
[2] P. G. Debenedetti, J. Phys.: Condens. Matter **15**, R1669 (2003).
[3] C. A. Angell, Annu. Rev. Phys. Chem. **55**, 559 (2004).
[4] T. Loerting and N. Giovambattista, J. Phys.: Condens. Matter **18**, R919 (2006).
[5] G. Malenkov, J. Phys.: Condens. Matter **21**, 283101 (2009).
[6] H. E. Stanley, C. A. Angell, U. Essmann, M. Hemmali, P. H. Poole, and F. Sciortino, Physica A **205**, 122 (1994).
[7] C. A. Angell, J. Shuppert, and J. C. Tucker, J. Phys. Chem. **77**, 3092 (1973).
[8] E. Mayer, J. Appl. Phys. **58**, 663 (1985).
[9] G. P. Johari, A. Hallbrucker, and E. Mayer, Nature (London) **330**, 552 (1987).
[10] R. S. Smith and B. D. Kay, Nature (London) **398**, 788 (1999).
[11] G. P. Johari, J. Phys. Chem. B **102**, 4711 (1998).
[12] O. Mishima, J. Chem. Phys. **100**, 5910 (1994).
[13] K. Winkel, W. Schustereder, I. Kohl, C. G. Salzmann, E. Mayer, and T. Loerting, in *Proceedings of the 11th International Conference on the Physics and Chemistry of Ice*, edited by W. F. Kuhs, (RSC, Dorchester, UK, 2007), pp. 641–648.
[14] A. K. Soper and M. A. Ricci, Phys. Rev. Lett. **84**, 2881 (2000).
[15] O. Mishima, J. Chem. Phys. **123**, 154506 (2005).
[16] R. Mancinelli, A. Botti, F. Bruni, M. A. Ricci, and A. K. Soper, Phys. Chem. Chem. Phys. **9**, 2959 (2007).
[17] R. Mancinelli, A. Botti, F. Bruni, M. A. Ricci, and A. K. Soper, J. Phys. Chem. B **111**, 13570 (2007).
[18] J. Holzmann, R. Ludwig, A. Geiger, and D. Paschek, Angew. Chem., Int. Ed. **46**, 8907 (2007).
[19] C. A. Angell, and E. J. Sare, J. Chem. Phys. **52**, 1058 (1970).
[20] K. Hofer, A. Hallbrucker, E. Mayer, and G. P. Johari, J. Phys. Chem. **93**, 4674 (1989).
[21] C. A. Angell, Chem. Rev. **102**, 2627 (2002); C. A. Angell, C. T. Moynihan, and M. Hemmati, J. Non-Cryst. Solids **274**, 319 (2000). Systems showing an Arrhenius temperature behavior of the viscosity are classified as strong glass formers.
[22] Y. Suzuki and O. Mishima, Phys. Rev. Lett. **85**, 1322 (2000).
[23] G. Fleissner, A. Hallbrucker, and E. Mayer, J. Phys. Chem. B **102**, 6239 (1998).
[24] K. Hofer, G. Astl, E. Mayer, and G. P. Johari, J. Phys. Chem. **95**, 10777 (1991).
[25] I. Kohl, L. Bachmann, A. Hallbrucker, E. Mayer, and T. Loerting, Phys. Chem. Chem. Phys. **7**, 3210 (2005).
[26] A. K. Soper, in *Proceedings of the Conference on Advanced Neutron Sources 1988*, IOP Conference Proceeding No. 97, edited by D. K. Hyer (Institute of Physics and Physical Society, London, 1989), p. 353. Detailed information on the SANDALS diffractometer can also be found at the web site: www.isis.stfc.ac.uk.
[27] See: www.isis.stfc.ac.uk/groups/disordered-materials/software.
[28] A. Botti, F. Bruni, R. Mancinelli, M. A. Ricci, F. Lo Celso, R. Triolo, F. Ferrante, and A. K. Soper, J. Chem. Phys. **128**, 164504 (2008).
[29] V. F. Sears, Neutron News **3**, 26 (1992).
[30] A. K. Soper, Chem. Phys. **202**, 295 (1996).
[31] A. K. Soper, Chem. Phys. **258**, 121 (2000).
[32] A. K. Soper, Mol. Phys. **99**, 1503 (2001).
[33] F. Bruni, M. A. Ricci, and A. K. Soper, J. Chem. Phys. **114**, 8056 (2001).
[34] A. Botti, F. Bruni, S. Imberti, M. A. Ricci, and A. K. Soper, J. Chem. Phys. **120**, 10154 (2004).
[35] A. Botti, F. Bruni, S. Imberti, M. A. Ricci, and A. K. Soper, J. Chem. Phys. **121**, 7840 (2004).
[36] S. Imberti, A. Botti, F. Bruni, G. Cappa, M. A. Ricci, and A. K. Soper, J. Chem. Phys. **122**, 194509 (2005).
[37] A. Botti, F. Bruni, M. A. Ricci, and A. K. Soper, J. Chem. Phys. **125**, 014508 (2006).
[38] S. E. McLain, S. Imberti, A. K. Soper, A. Botti, F. Bruni, and M. A. Ricci, Phys. Rev. B **74**, 094201 (2006).

[39]R. Mancinelli, A. Sodo, F. Bruni, M. A. Ricci, and A. K. Soper, J. Phys. Chem. B **113**, 4075 (2009).
[40]A. Botti, S. E. Pagnotta, F. Bruni, and M. A. Ricci, J. Phys. Chem. B **113**, 10014 (2009).
[41]F. Bruni, M. A. Ricci, and A. K. Soper, in *Conference Proceedings*, edited by M. Nardone and M. A. Ricci (Italian Physical Society, Bologna, 2000), pp. 37–48.
[42]A. K. Soper, J. Phys.: Condens. Matter **19**, 415108 (2007).
[43]H. J. C. Berendsen, J. R. Grigera, and T. P. Straatsma, J. Phys. Chem. **91**, 6269 (1987).
[44]The potential parameters for Cl^- have been taken from A. K. Soper and K. Weckstrom, J. Chem. Phys. **124**, 180 (2006); those for Li^+ from Ref. 36, by changing the ionic charge to $+1$, in order to get a neutral sample.
[45]M. A. Ricci, F. Bruni, and A. Giuliani, Faraday Discuss. **141**, 347 (2009).
[46]D. T. Bowron, J. L. Finney, A. Hallbrucker, I. Kohl, T. Loerting, E. Mayer, and A. K. Soper, J. Chem. Phys. **125**, 194502 (2006).
[47]A. Botti, F. Bruni, A. Isopo, M. A. Ricci, and A. K. Soper, J. Chem. Phys. **117**, 6196 (2002).
[48]The number of first neighbours of an i atom is calculated by averaging over a large number of configurations the number of $i - j$ pairs found in the simulation box within a distance equal to the first minimum of the $g_{ij}(r)$. The reported uncertainty is the standard deviation.
[49]A. P. Lyubartsev, K. Laasonen, and A. Laaksonen, J. Chem. Phys. **114**, 3120 (2001).
[50]J. F. Jal, A. K. Soper, P. Carmona, and J. Dupuy, J. Phys.: Condens. Matter **3**, 551 (1991).
[51]H. Kanno, J. Phys. Chem. **91**, 1967 (1987).
[52]Y. Suzuki and O. Mishima, J. Chem. Phys. **117**, 1673 (2002).
[53]Y. Yoshimura and H. Kanno, J. Phys.: Condens. Matter **14**, 10671 (2002).
[54]Y. Suzuki and O. Mishima, J. Phys.: Condens. Matter **21**, 155105 (2009).
[55]O. Mishima, J. Chem. Phys. **126**, 244507 (2007).
[56]K. Winkel, M. S. Elsaesser, E. Mayer, and T. Loerting, J. Chem. Phys. **128**, 044510 (2008).
[57]K. Winkel, M. Bauer, E. Mayer, M. Seidl, M. Elsaesser, and T. Loerting, J. Phys.: Condens. Matter **20**, 494212 (2008).